International Journal of Heat and Mass Transfer 52 (2009) 3518–3524

Contents lists available at ScienceDirect

International Journal of Heat and Mass Transfer

journal homepage: www.elsevier.com/locate/ijhmt

Potential tissue damage from transcutaneous recharge of neuromodulation implants

Ryan D. Lovik [a], John P. Abraham [b,*], Ephraim M. Sparrow [a]

[a] Department of Mechanical Engineering, University of Minnesota, Minneapolis, MN 55455, USA
[b] School of Engineering, University of St. Thomas, St. Paul, MN 55105, USA

ARTICLE INFO

Article history:
Received 24 January 2009
Received in revised form 3 March 2009
Accepted 3 March 2009
Available online 18 April 2009

Keywords:
Neuromodulation
Magnetic-field heating
Implant
Bio-heat equation
Tissue-damage integral
Hot-spot tissue temperature
Necrosis

ABSTRACT

The magnetic-field-driven heat generation in neuromodulation systems consisting of implanted and skin-surface-mounted components gives rise to the potential of discomfort, cell damage, and possible necrosis. The skin-surface-mounted component, commonly termed the *antenna*, serves the function of the primary of a transformer, and the implant is the secondary. Heating occurs in both of these components during the recharging of a battery situated in the implant. Previously reported experimental data for the heat generation characteristics of three commercially available neurostimulation systems has been enhanced by further experiments carried out as part of this investigation. A numerical simulation of the temperature distribution in tissue beds adjacent to the implant and the antenna has been performed here. The aggregated data have been used as input information to a bio-heat-transfer model which yields both the spatial and temporal variations of the temperature field. It was found that during long-duration recharging periods, the temperature of the tissue rises in response to the heat generation. This information enables the identification of the magnitude and location in the tissue of the hot-spot temperature. The temporal temperature variation at the hot spot was employed in conjunction with a tissue-damage integral to identify the possibility of cell damage and/or necrosis. It was found that two of the three investigated neuromodulation systems did not give rise to temperature levels that may cause tissue damage. However, the third of the systems caused temperatures of sufficient elevation so that for recharging periods on the order of 2 h, necrosis was found to be likely in situations where heat transfer is suppressed at the surface of the skin.

1. Introduction

Safety considerations have evoked considerable recent interest in the interaction of external magnetic fields with implanted metallic objects in the human body. One application which has been regarded as critical with respect to the general impact of this interaction is the use of MRI as a diagnostic tool. A second situation where a similar interaction occurs is when an implant is empowered by a magnetic field dispersed by an antenna situated on the skin surface in the near proximity of the implant. The externally applied magnetic field penetrates the tissue and induces eddy currents in the metallic implant or other structures. The induced currents, in turn, produce Ohmic heating. In addition, possible chemical reactions due to the recharging process may also produce heat. The concern is that Ohmic and chemically produced heating may give rise to local elevated temperatures which may cause tissue necrosis. The current literature dealing with this heating phenomenon is well documented [1–12]. These papers run the gamut from MRI-based heating to antenna-based heating. In addition to the aforementioned thermal effect, the external magnetic field may also interfere with the primary function of the implanted device, an occurrence which has been reported in literature of which [13–16] are representative.

The investigation to be described here seeks to quantify the impact of the heating effect caused by the interaction of an externally applied magnetic field and an implant. The specific situation to be considered is a neurostimulation implant which is recharged by a skin-surface-mounted antenna. The three neurostimulation devices investigated here are the Medtronic Restore, the ANS Eon, and the Boston Scientific Precision. In a previous paper [17], careful *in vitro* experiments were performed to obtain the rate of energy transfer from the surfaces of the implant to the adjacent tissue. These rates, taken from Ref. [17] are 233, 670, and 441 mW, respectively, for the Medtronic Restore, the ANS Eon, and the Boston Scientific Precision. In addition, the experiments provided the following data: 200, 343, and 931 mW, respectively, for the Medtronic Restore, the ANS Eon, and the Boston Scientific Precision for the energy transfer rate from the antenna surfaces to its environment.

In the work to be described here, further experiments were performed to quantify the rates of energy transfer specific to each

* Corresponding author. Tel.: +1 651 962 5766; fax: +1 651 962 6419.
E-mail address: jpabraham@stthomas.edu (J.P. Abraham).

0017-9310/$ - see front matter © 2009 Elsevier Ltd. All rights reserved.
doi:10.1016/j.ijheatmasstransfer.2009.03.010

Nomenclature

A	pre-exponential thermal injury constant
c	specific heat
E_A	activation energy for thermal injury
k	thermal conductivity
r	radial coordinate
$\bar{R}$	universal gas constant
S	volumetric rate of energy generation by metabolism
t	time
T	temperature
T_a	arterial temperature
z	axial coordinate
Symbols	
ρ	density
τ	integration variable
Ω	thermal injury index
ω	volumetric rate of blood perfusion per unit volume of tissue

of the principal surfaces of the implant. These experiments were performed with the respective implants suspended in air. To avoid uncertainties attributable to random air currents, the suspended implant was partially shrouded. A heat-flux sensor was affixed to each of the principal surfaces of the implant. These sensors provided a direct reading of the heat flux passing from the surface to the surrounding environment. To create a situation in which heat was generated within the implant, the antenna that corresponded to each implant was suspended parallel to the implant and separated from it by a distance of one cm. Once the set-up had been created, the antenna was activated to initiate and maintain the recharging of the implant. When steady state had been established, the heat fluxes passing from the respective principal surfaces to the air environment were read electronically. The outcome of these experiments yielded the percentage of the total heat transfer rate leaving the principal surfaces that is attributable to each principal surface. For the Medtronic Restore, 29% of the heat transfer from principal surfaces was attributed to the surface that faces the skin. The corresponding numbers for the ANS Eon and Boston Scientific Precision implants are 44% and 37%, respectively. The percentages passing through the surface that faces the deeper portions of the tissue bed are 71, 56, and 63.

These data, together with those of Ref. [17], were then used as the basis of a numerical simulation model of the energy transfers within the tissue. To achieve a high level of accuracy for the numerical predictions, the detailed internal structure of the antennas was carefully taken into account. By this detailed modeling, it was possible to precisely identify the energy transfers from the respective bounding surfaces of the antennas and the evolution of the temperature field within the tissue.

The investigation was performed for three different neuromodulation systems, the Medtronic Restore, the ANS Eon, and the Boston Scientific Precision. For each of these devices, the temperature distribution in the tissue in the neighborhood of the implant and the antenna was determined. Careful attention was given to the specification of the boundary conditions for the analysis. Specifically, clothing worn over the antenna plus heat transfer by convection and radiation to the environment formed the basis of one of the employed boundary conditions. Another boundary condition was based on the patient oriented so that the antenna was in contact with an insulating material such as that of a sofa or a mattress.

The simulation was performed for transient operation, with the transient being initiated by the activation of the antenna's magnetic field. The period of the heating was extended over a duration of 2 h. This period of application of the device is believed to cover most practical utilizations.

The special focus of the work was to investigate conditions which could give rise to local tissue necrosis during the recharging of the aforementioned neuromodulation devices.

2. Physical and mathematical models

A schematic display of the physical model is conveyed in Fig. 1. The model is, in fact, axisymmetric, and a cut along a diametril plane (a vertical plane which is cut through a diameter) is exhibited in the figure. The tissue bed is characterized as a four-layer assemblage, encompassing the skin, fat, fascia, and muscle layers. The respective thicknesses of these layers are 2, 30, 1, and 25 mm. These thicknesses were selected on the basis of a consultative discussion with a plastic surgeon [18]. The selected thickness of the fat layer was sufficiently great to fully encompass the implant. In view of the fact that the fat layer has the lowest thermal conductivity and the lowest blood perfusion rate among all the others, the positioning of the implant in that layer necessarily gives rise to an upper bound on the temperature at the interface of the implant and the tissue. The implant depth, which is defined in Fig. 1, is one cm for all the investigated implants. The thicknesses of the implants are 13.9, 15.6, and 10.5 mm for the Medtronic Restore, ANS Eon, and Boston Scientific Precision, respectively.

Fig. 1 is, in fact, a representation of the volume in which the numerical solutions were performed. All of the dimensions of that space have been conveyed in the foregoing, aside from the radius which defines the outer edge and the dimensions of the antenna. The outer radius of the solution space was taken to be two and a half times the radius of the antenna. The antenna radii are 39.1, 40.3, and 35.6 mm, respectively, for the Medtronic Restore, ANS Eon, and Boston Scientific Precision devices.

A complete listing of the properties of the selected tissue layers is provided by Table 1. The properties were chosen after an exten-

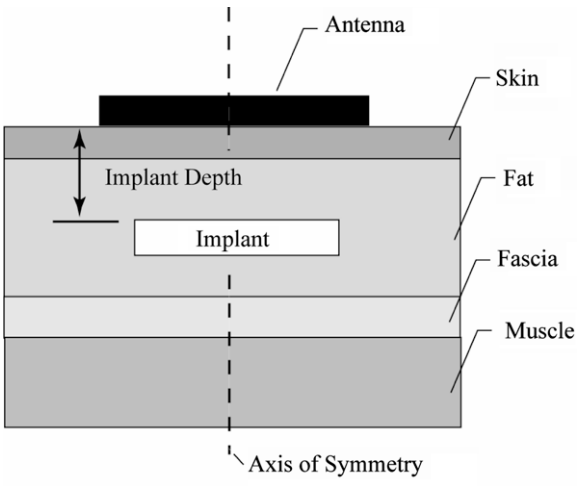

Fig. 1. Schematic diagram of the system to be investigated, showing the four tissue layers, the skin-surface-mounted antenna, and the implant.

sive review of the literature and may be regarded as representative of the non-pathological patients.

The energy transfers in the tissue bed can be modeled by applying the first law of thermodynamics. That law is, in fact, a balance of the inflows and outflows of energy into a control volume. The energy flows that are considered are: (a) heat conduction, (b) perfusion-carried energy, and (c) metabolic heat generation. When these various transports are in balance, a steady state is achieved. The most commonly accepted form of the first law for biological thermal transport is the Pennes equation [28]. This model has provoked a considerable amount of controversy over many decades. Despite this, it has been demonstrated to be viable by comparisons between the predictions of the model and experimental data. The Pennes equation is

$$\rho c\frac{\partial T}{\partial t}=k\frac{\partial^2 T}{\partial z^2}+\frac{k}{r}\frac{\partial}{\partial r}\left(r\frac{\partial T}{\partial r}\right)+(\rho c)_b\omega(T_a-T)+S. \tag{1}$$

This equation is written for an axisymmetric model, justifying the use of cylindrical coordinates. Also worthy of note is that it takes account of unsteady temperature variations. The solutions to be obtained will encompass not only the transient state but also will provide the steady state which occurs as the limit as time increases.

In this equation, the thermal physical properties are k, ρ, and c, which are the thermal conductivity, the density, and the specific heat of tissue, respectively, and ρ_b, c_b, which are, respectively, the density and specific heat of blood. The specific rate of blood flow is represented by ω which has units of $(m^3/s)/(m^3)$. The numerator of this unit cluster is the volumetric flow rate, while the denominator represents the volume of tissue through which the blood is perfusing. Also appearing in Eq. (1) is a baseline temperature T_a. According to Pennes, T_a represents the temperature of the arterial blood which perfuses through the tissue. Metabolic heat generation is denoted by S, which corresponds to a volumetric heat source. The dependent variable is the temperature T, which is a function of the axial and radial coordinates, r and z, respectively. Aside from the independent and dependent variables, numerical values of the other quantities that appear in (1) are listed in Table 1, except for blood, for which $\rho_b = 1000\ kg/m^3$ and $c_b = 4000\ J/(kg\ K)$.

The goal of this investigation is to solve Eq. (1) to obtain the maximum temperatures in the tissue caused by the heat generation in the implant and the antenna. The presence of those devices is not reflected in Eq. (1). The heat generation within the implant will enter the problem as a boundary condition. On the other hand, the antenna will be modeled in its own right, and the energy transfers within it are governed by a form of the first law that differs from Eq. (1). In fact, in view of the complicated geometry of the internal parts of the antenna, it was necessary to solve a separate governing equation for each part. If the subscript i is used to identify each part, then the relevant form of the first law is

$$(\rho c)_i\frac{\partial T_i}{\partial t}=k_i\frac{\partial^2 T_i}{\partial z^2}+\frac{k_i}{r}\frac{\partial}{\partial r}\left(r\frac{\partial T_i}{\partial r}\right)+S_i. \tag{2}$$

In those parts of the antenna where heat generation occurs due to Ohmic heating, the volumetric heat source term S_i has a constant value. On the other hand, certain parts of the antenna merely act as heat conductors, and in those parts, $S_i = 0$. To illustrate the complexity of the interior of an antenna, Fig. 2 has been prepared. It is a vertical cut through the antenna showing a cross-section. This antenna is specific to the Medtronic Restore device. In this cross-sectional view, 10 different materials are identified. Some of these materials appear in more than one location in the antenna. Of particular note is the heat-generating element as indicated in the diagram (part 1). In the particular antenna that is illustrated, there are 15 separate parts, each of which necessitates the solution of a separate differential equation such as Eq. (2). Similar details were obtained for the other two devices but are not shown for brevity.

Inspection of Fig. 2 reveals the presence of air gaps. Since the bounding surfaces of the air gaps are necessarily at different temperatures, it is appropriate to consider the possibility of natural convection occurring in these gaps. This possibility was examined by making use of the Rayleigh number criteria for the onset of flow in both horizontal and vertical enclosures. For all of the air gaps that occur in the antenna pictured in Fig. 2, it was found that the Rayleigh number was well below that for the onset of flow. This same issue arose for the Boston Scientific Precision antenna. A calculation of the Rayleigh number for the air gap that exists in that antenna also gave rise to a value below the critical.

To complete the specification of the problem, it is necessary to provide boundary conditions and conditions of continuity at interfaces. With reference to Fig. 1, the exposed surfaces of the antenna and the exposed surface of the skin were assigned continuous boundary conditions. Two boundary conditions were considered. One of these took account of convection to the surrounding ambient in the presence of garments covering the antenna and the skin surface. The thermal resistances of the garments and the convective resistance of the air were lumped into an overall heat transfer coefficient. A second boundary condition was based on modeling a situation where the antenna and skin surface interfaced with a thick insulating material such as an upholstered chair or a bed. For that case, an adiabatic boundary condition was imposed.

At the interface between the base of the antenna and the contiguous skin surface, perfect contact was assumed. At the outboard edges of the solution domain that are shown in Fig. 1, it was assumed that the influence of the presence of both the antenna and the implant had died away. Consequently, an adiabatic boundary condition was appropriate. With regard to the bottom of the tissue bed, it was uncertain what would be the proper boundary condition, since the overall depth of the bed was unlikely to be thick enough to impose the core temperature. This uncertainty led to the selection of the adiabatic condition, whose adoption would give rise to temperatures that correspond to an upper bound on the actual temperature field. However, subsequent computation experience demonstrated that the use of this boundary condition gave rise to temperature increases on the order of 0.2 °C. At all other interfaces, continuity of temperature and heat flux was required.

As noted earlier, the implant was not included in the solution domain. Rather, on the basis of experiments reported in Ref. [17] and extended as part of the present research, the heat flux leaving the surfaces of the implant and entering the tissue were known quantities. These known heat fluxes were applied as boundary con-

Table 1
Properties of the tissue layers.

Tissue	Layer thickness (mm)	Thermal conductivity (W/m K)	Density (kg/m^3)	Specific heat (J/kg K)	Median blood perfusion rate (1/s)	Metabolic heating rate (W/m^3)
Skin	2	0.45 [19]	1100 [21]	3500 [19]	0.0018 [23]	1300 [25]
Fat	30	0.2 [20]	960 [21]	2500 [24]	0.000425 [26]	250 [25]
Fascia	1	0.23 [21]	1000 [21]	3900 [21]	0.000425 [26]	250 [25]
Muscle	25	0.5 [22]	1040 [21]	3600 [24]	0.0005 [27]	500 [25]

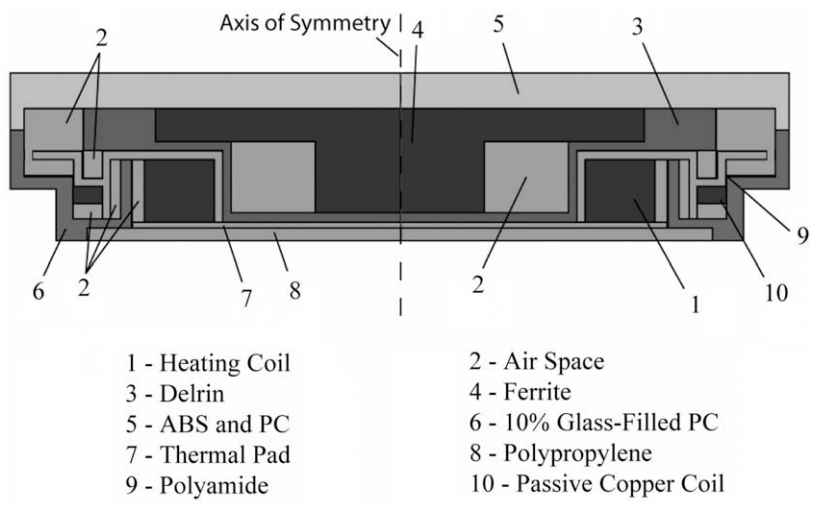

Fig. 2. Vertical cut through an antenna illustrating the presence of numerous separate parts.

ditions at the interface of the implant and the contiguous tissue. The data provided by Weinmann and Sparrow [17] were the total rate of heat transfer from all faces of the implant to its surroundings. Additional experiments performed here utilizing heat flux sensors enabled accurate determinations of the separate heat flow rates from the two principal surfaces. In particular, these experiments showed that for the Restore, Eon, and Precision, the percentages of the total energy leaving the implant that is transferred from the skin-facing surface are 29, 44, and 37, respectively.

The actual numerical computations were performed within the framework of ANSYS 11.0. The accuracy of the numerical solutions was validated by a mesh independence study. Meshes consisting of 75,600 and 108,000 elements were employed for this study. The temperature maximum was monitored for these two mesh densities, and it was found that agreement prevailed to within 0.01 °C for all times during the transient process.

3. Results and discussion

The result of most immediate interest is the magnitude of the hot-spot temperature within the tissue bed and its location. This information is conveyed in Figs. 3–5, respectively, for the Boston Scientific Precision, ANS Eon, and Medtronic Restore devices. The results displayed in these figures correspond to a time following 1 h of recharging of the respective devices. Also, the thermal boundary condition at the exposed surfaces (the outer surface of clothing covering the skin and the antenna) was natural convection and radiation to the surroundings. In interpreting the results conveyed by these figures, it is well to keep in mind that an axisymmetric model has been used for the numerical simulation. To provide a realistic portrayal, the figures display a 180° revolution of the basic two-dimensional geometry.

The figures display color contour diagrams of the temperatures both within the tissue and the antenna. The temperature levels are correlated to the color scale that is situated beneath the contour diagram. Note that a common color scale is used for all of these figures. From an overview of the figures, it is clear that the highest hot-spot temperature within the tissue (45.6 °C) is attained when the Boston Scientific Precision device is employed. The hot-spot temperature associated with the ANS Eon is somewhat lower (41.1 °C) than that of the Boston Scientific Precision device. The lowest of the hot-spot temperatures is that with the use of the Medtronic Restore device (39.2 °C). With regard to the location of these hot-spot temperatures, it can be seen that for the Precision device, the location is at the skin surface. On the other hand, for both of the other two devices, the hotspot is located adjacent to the bottom surface of the implant.

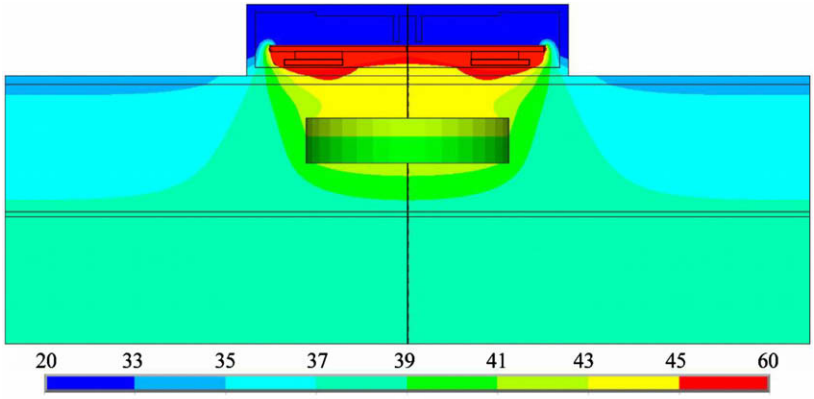

Fig. 3. The temperature distribution (°C) associated with the Boston Scientific Precision device after 1 h of recharging. Note that temperatures above 50 °C are encountered in the antenna and not in the tissue. The maximum tissue temperature is 45.6 °C. The apparent discontinuity between the temperatures of 33 and 45 °C in the antenna is due to the very high thermal resistance of an air gap.

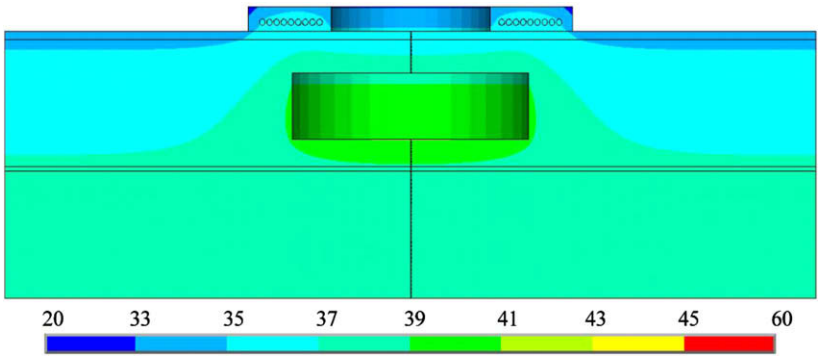

Fig. 4. The temperature distribution (°C) associated with the ANS Eon device after 1 h of recharging. The maximum temperature in the tissue is 41.1 °C.

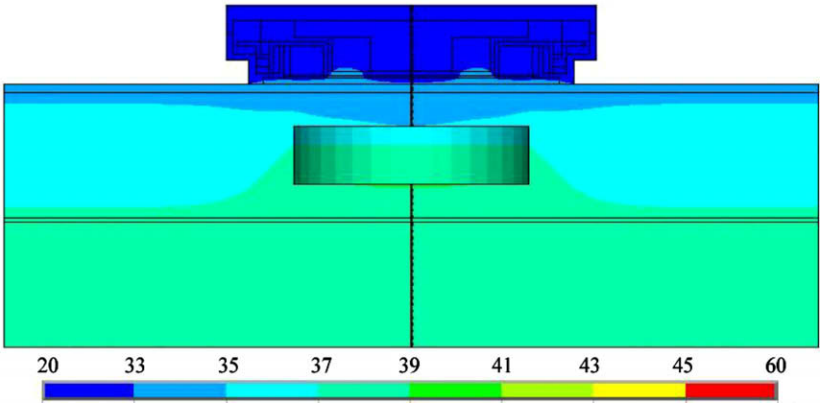

Fig. 5. The temperature distribution (°C) associated with the Medtronic Restore device after 1 h of recharging. The maximum tissue temperature is 39.2 °C.

Among the three aforementioned hot-spot temperatures, only that for the Precision device might possibly suggest cell damage. It is known that cell necrosis is a function not only of temperature level, but it also depends on the time duration at which the elevated temperature exists. The issue of cell necrosis will be treated in greater depth shortly when time durations of various extents are considered.

Color contour diagrams similar in content to Figs. 3–5 were examined for the thermal boundary condition of no heat transfer at the exposed surfaces of the skin and the antenna. That inspection indicated only small differences from the contours that were exhibited for the case of surface convection. Therefore, the contour diagrams for the adiabatic case will not be presented here.

More detailed information about the timewise variation of the hot-spot temperatures is conveyed in Figs. 6–8. In each of these figures, the hot-spot temperature is plotted as a function of time for each of the devices being considered. The time span for which results are presented is 60 min. Fig. 6 shows results for the three devices in the presence of surface convection. These results are delineated by curves of different line types. The highest temperatures achieved during the 1-h recharging period are those for the Boston Scientific Precision. The hot-spot location for that device shifted from the bottom surface of the implant at early times to the skin–antenna interface at later times. This change of site is responsible for the change of slope of the curve for this device. The intermediate temperatures are those for the ANS Eon, the site of which was the bottom surface of the implant. The lowest of the hot-spot temperatures are those for the Medtronic Restore. At relatively short times during the recharging period, the hot-spot temperatures of the various devices differ by approximately 3 °C, while at larger times differences as large as 6.5 °C are in evidence.

The counterpart of Fig. 6 which conveys similar results for the case of no heat transfer at the exposed surfaces is Fig. 7. Examination of these figures indicates only minor differences in detail. Over all, the maximum deviations in the hot-spot temperatures for the two thermal boundary conditions are, at most, one degree Celsius.

Next, attention is turned to a display of the outcome of a sensitivity study in which the blood perfusion rate was varied by ±50% around the nominal value that was listed in Table 1. The hot-spot temperatures corresponding to the three perfusion rates for each of the three devices are exhibited in Fig. 8. In that figure, three clusters of curves are shown, with the uppermost cluster corresponding to the Precision device, the middle to the ANS Eon, and the

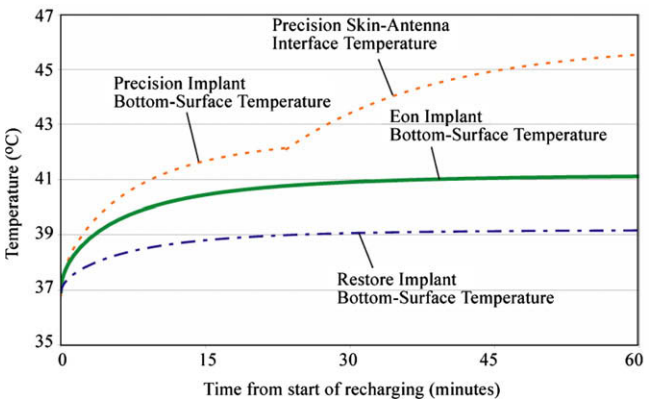

Fig. 6. Hot-spot temperatures for all three devices corresponding to a 20 °C convective environment.

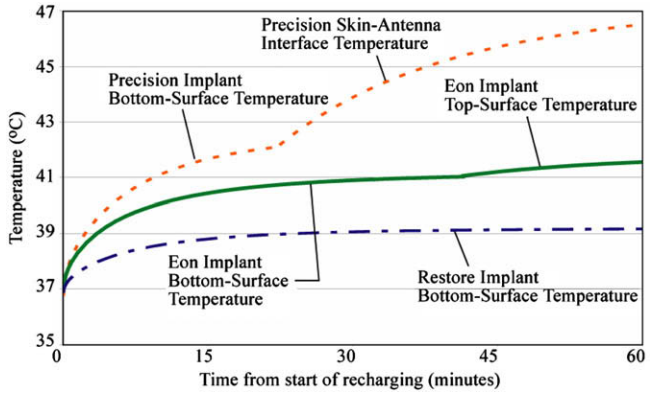

Fig. 7. Hot-spot temperatures for all three devices corresponding to an adiabatic environment.

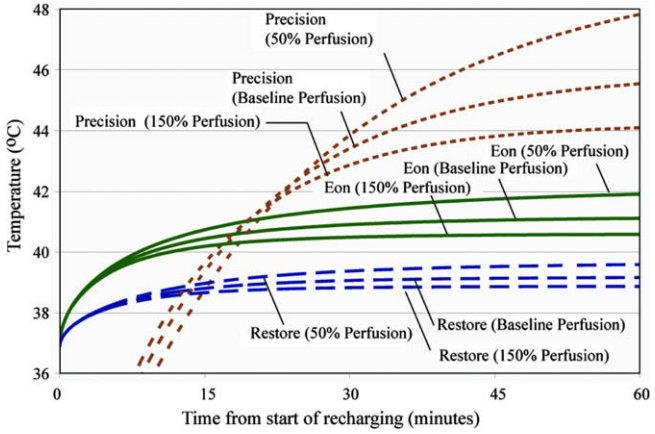

Fig. 8. Dependence of the hot-spot temperatures on the blood perfusion rate.

lower to the Medtronic Restore. For the latter two devices, the curves are consistently ordered with respect to the blood perfusion rate, with the highest hot-spot temperatures corresponding to the lowest perfusion rate and the lowest hot-spot temperature belonging to the highest perfusion. With respect to the Precision device, the just-described ordering of the curves also describes the results for times greater than 20 min. At lesser values of time, the ordering is reversed. It is especially important to note that both the ANS Eon and the Medtronic Restore give rise to hot-spot temperatures that are not very sensitive to the perfusion rate. On the other hand, the Boston Scientific Precision is much more sensitive to perfusion, especially at relatively long recharging times. For example, for a recharging time of 60 min, the perfusion-caused spread in the hot-spot temperature is approximately 4 °C.

It is convenient to summarize the key results of the foregoing paragraphs in tabular form. This information is provided by Table 2. The table lists the hot-spot temperatures for each of the investigated devices at 15, 30, 45, and 60 min of recharging. Also listed in the table are the results for the two boundary conditions, convective and adiabatic. The distinction between these results is made by placing the adiabatic-based temperatures in parentheses. The results exhibited in the table correspond to the properties that are listed in Table 1.

Inspection of the table confirms the observations that have been reported from the discussions of the figures. Among the devices, the highest temperatures are those for the Boston Scientific Precision, the intermediate temperatures correspond to the ANS Eon,

Table 2
Summary of the hot-spot temperature results at different durations of recharging (°C).

Device	Duration of recharging (min)			
	15	30	45	60
Precision	41.7 (41.7)	43.4 (43.9)	44.9 (45.7)	45.6 (46.5)
Eon	40.4 (40.4)	40.9 (40.9)	41.1 (41.2)	41.1 (41.6)
Restore	38.8 (38.8)	39.1 (39.1)	39.1 (39.1)	39.2 (39.2)

Table 3
Cumulative thermal injury imparted to hot-spot tissue locations due to device recharging.

Device	Duration of recharging (h)	
	1	2
Boston Scientific Precision	0.071 (0.15)	0.35 (1.0)
ANS Eon	0.0023 (0.0024)	0.0058 (0.0059)
Medtronic Restore	0.00041 (0.00041)	0.00092 (0.00093)

while the lowest temperatures are those for the Medtronic Restore. The table also confirms the minor differences that are attributable to the differences in the thermal boundary conditions, convective versus adiabatic.

The impact of the temperatures displayed in Table 2 on possible cell necrosis will now be considered. To this end, use is made of the Henriques–Moritz [29] cell injury criterion, which is

$$\Omega(t) = A \int_0^t e^{-E_A/(\overline{R}T)} d\tau. \tag{3}$$

In this equation, E_A is the activation energy, $\overline{R}$ is the universal gas constant, τ is the variable of integration, and A is the so-called pre-exponential constant. The values of E_A and A are specific to each of the tissue layers. Those for skin, $A = 2.20 * 10^{124}\ s^{-1}$ and $E_A = 7.84 * 10^5$ J/mol, were used for the evaluation of the integral [30]. The computed timewise temperatures $T(\tau)$ were introduced into the integrand and the integration was performed numerically. The results for Ω are listed in Table 3. The table exhibits Ω values for device recharging times of 1 and 2 h. Separate results are listed for the two considered thermal boundary conditions, convection to an environment at 20 °C and adiabatic exposed surfaces. The results for the latter are delineated by parentheses.

There is a consensus that cell necrosis occurs for values of Ω on the order of one. In this light, it appears that only for the case of the Boston Scientific Precision device is there a danger of necrosis for recharging periods on the order of 2 h. For this device operating at shorter durations and for all the other devices, it appears that no cell damage occurs. It is noteworthy that both the Medtronic Restore and the ANS Eon yield very low values of Ω for all of the time durations considered. This observation suggests that they are absolutely safe with regard to thermal injury of tissue with regard to the investigated conditions.

4. Concluding remarks

The thermal implications of biomedical implants activated by magnetic fields have been investigated here by means of numerical simulation making use of experimentally determined device heat generation measurements. The specific type of implant that motivated this investigation is neuromodulators. In essence, the implant is the secondary of a transformer, while the primary (the antenna) is situated on the skin surface. The specific implant–antenna arrangement considered here is a separation of the two components by a tissue layer of 1 cm. The original experiments obtained data for the rate at which heat is transferred from all of

the surfaces of the respective implant devices to the surroundings. Further experiments performed here determined the fractions of that heat transfer rate attributable to the respective principal surfaces of each device.

The numerical simulations, based on these inputs and on thermophysical properties and perfusion rates from the literature, predicted the magnitude and location of the maximum temperature created in the tissue as a result of the presence of the implant and the antenna. These so-called hot-spot temperatures were determined for three of the most-used neuromodulators: (a) Boston Scientific Precision, (b) ANS Eon, and (c) Medtronic Restore.

The critical heating period for these devices is that during which recharging of the implant's battery is taking place. For durations of the recharging between 30 and 60 min, the predicted hot-spot temperatures are 43.4–44.9 °C for the Precision, 40.9–41.1 °C for the Eon, and 39.1–39.2 °C for the Restore. These temperatures correspond to the thermal boundary condition whereby there is convective heat transfer to a 20 °C environment. For the other investigated situation, where the thermal boundary condition was specified to be adiabatic, the corresponding temperatures are 43.9–46.5 °C for the Precision, 40.9–41.6 °C for the Eon, and 39.1–39.2 °C for the Restore. These temperature levels suggest that, at least for the case of the Precision device, there is a possibility of tissue damage.

To quantify the possibility of tissue damage, the Henriques–Moritz tissue-damage integral was used to combine the effects of temperature level and duration of the recharging period. For a recharging period of 1 h, the damage integral for all of the three devices yielded numbers much less than one, which is the accepted indicator of tissue necrosis. If the heating period encompassed a 2-h duration, the damage integral for both the Eon and Restore produce values which are, once again, much smaller than one. The values of the damage integral for the Precision device for the 2-h recharging are 0.35 and 1.0, respectively, for the convective and adiabatic boundary conditions (a worst case). This outcome suggests that caution be exercised when using this device.

Acknowledgement

Financial support for this project was provided by Medtronic, Incorporated.

References

[1] G. Calcagnini, M. Triventi, F. Censi, R. Mattei, P. Bartolini, W. Kainz, H.I. Bassen, In vitro investigation of pacemaker lead heating induced by magnetic resonance imaging: role of implant geometry, J. Magn. Reson. Imaging 28 (2008) 879–886.
[2] S.A. Mohsin, N.M. Sheikh, U. Saeed, MRI induced heating of deep brain stimulation leads: effect of the air–tissue interface, Progr. Electromagn. Res. 8 (2008) 81–91.
[3] S.M. Park, R. Kamondetdacha, J.A. Nyenhuis, Calculation of MRI-induced heating of an implanted medical lead wire with an electric field transfer function, J. Magn. Reson. Imaging 26 (2007) 1278–1285.
[4] K. Yassi, F. Ziane, E. Bardinet, M. Moinard, B. Veyret, J.F. Chateil, Evaluation of the risk of overheating and displacement of orthodontic devices in magnetic resonance imaging, J. Radiol. 88 (2007) 263–268.
[5] H.I. Bassen, W. Kainz, G. Mendoza, T. Kellom, MRI-induced heating of selected thin wire metallic implants – laboratory and computational studies – findings and new questions raised, Minim. Invas. Ther. Allied Technol. 15 (2006) 76–84.
[6] E. Matte, G. Calcagnini, M. Triventi, F. Censi, P. Bartolini, W. Kainz, H.I. Bassen, MRI induced heating of pacemaker leads: effect of temperature probe positioning and pacemaker placement on lead tip heating and local SAR, in: Annual International Conference of the IEEE Engineering in Medicine and Biology Society, vol. 1, 2006, pp. 1889–1892.
[7] J.A. Nyenhuis, S.M. Park, R. Kamondetdacha, A. Amjad, F.G. Shellock, A.R. Rezai, MRI and implanted medical devices: basic interactions with an emphasis on heating, IEEE Trans. Device Mater. Reliab. 5 (2005) 467–479.
[8] U.D. Nguyen, J.S. Brown, I.A. Chang, J. Krycia, M.S. Mirotznik, Numerical evaluation of heating of the human head due to magnetic resonance imaging, IEEE Trans. Biomed. Eng. 51 (2004) 1301–1309.
[9] W.R. Nitz, A. Oppelt, W. Renz, C. Manke, M. Lenhart, J. Link, On the heating of linear conductive structures as guide wires and catheters in interventional MRI, J. Magn. Reson. Imaging 13 (2001) 105–114.
[10] M.F. Dempsey, B. Condon, D.M. Hadley, Investigation of the factors responsible for burns during MRI, J. Magn. Reson. Imaging 13 (2001) 627–631.
[11] F.G. Shellock, Radiofrequency energy-induced heating during MR procedures: a review, J. Magn. Reson. Imaging 12 (2000) 30–36.
[12] J.A. Nyenhui, A.V. Kildishev, T.W. Athey, J.D. Bourland, K.S. Foster, G.P. Graber, Heating near implanted medical devices by the MRI RF-magnetic field, in: Digest of the International Magnetic Conference, 1999, BQ-12.
[13] O.G. Anfinsen, R.F. Bernsten, H. Aass, E. Kongsgaard, J.P. Amlie, Implantable cardioverter defibrillator dysfunction during and after magnetic resonance imaging, Pacing Clin. Electrophysiol. 25 (2002) 1400–1402.
[14] S.L. Pinski, R.G. Trohman, Interference in implanted cardiac devices, part II, Pacing Clin. Electrophysiol. 25 (2002) 1496–1509.
[15] M. Niehus, J. Tebbenjohanns, Electromagnetic Interference in patients with implanted pacemakers or cardioverter-defibrillators, Heart 86 (2001) 246–248.
[16] S. Achenbach et al., Effects of MRI on cardiac pacemakers and electrodes, Am. Heart J. 134 (1997) 467–473.
[17] J.J. Weinmann, E.M. Sparrow, Heat flow from neuromodulation systems into surrounding media, Neuromodulation 12 (2009), in press.
[18] January 25, 2008, Meeting with Dr. Marie Clair Buckley.
[19] S.C. Jiang, N. Ma, H.J. Li, X.X. Zhang, Effects of thermal properties and geometrical dimensions on skin burn injuries, Burns 28 (2002) 713–717.
[20] M.L. Cohen, Measurement of the thermal properties of human skin. A review, J. Invest. Dermatol. 69 (1977) 333–338.
[21] F.A. Duck, Physical properties of tissue, A Comprehensive Reference Book, Academic Press, London, 1990.
[22] J.W. Valvano, J.T. Allen, H.F. Bowman, The simultaneous measurement of thermal conductivity thermal diffusivity and perfusion in small volumes of tissue, ASME 81-WA/HT-21, 1981.
[23] J.M. Johnson, G.L. Brengelmann, J.R.S. Hales, P.M. Vanhoutte, C.B. Wenger, Regulation of the cutaneous circulation, Fed. Proc. 45 (1986) 2841–2850.
[24] T. Kobayash, T. Nemoto, A. Kamiya, T. Togawa, Improvement of deep body thermometer for man, Ann. Biomed. Eng. 3 (1975) 181–188.
[25] D. Brajkovic, M.B. Ducharme, Confounding factors in the use of the zero-heat-flow method for non-invasive muscle temperature measurement, Eur. J. Appl. Physiol. 94 (2005) 386–391.
[26] R.H. Fox, A.J. Solman, A new technique for monitoring the deep body temperature in man from the intact skin surface, J. Physiol. 212 (1971) 8P–10P.
[27] R.H. Fox, A.J. Solomon, R. Isaacs, A.J. Fry, I.C. MacDonald, A new method for monitoring deep body temperatures from the skin surface, Clin. Sci. 44 (1973) 81–86.
[28] H.H. Pennes, Analysis of tissue and arterial blood temperatures in the resting human forearm, J. Appl. Physiol. 85 (1948) 5–34.
[29] F.C. Henriques, A.R. Moritz, Studies of thermal injury I: the conduction of heat to and through the skin and the temperatures attained therein. A theoretical and experimental investigation, Am. J. Pathol. 23 (1947) 531–549.
[30] J.A. Weaver, A.M. Stoll, Mathematical model of skin exposed to thermal radiation, Aerospace Med. (1969) 24–30.